Chemical Geology 417 (2015) 261–272

Contents lists available at ScienceDirect

Chemical Geology

journal homepage: www.elsevier.com/locate/chemgeo

Dynamic evolution of the Ediacaran ocean across the Doushantuo Formation, South China

Tao Han, Haifeng Fan *

State Key Laboratory of Ore Deposit Geochemistry, Institute of Geochemistry, Chinese Academy of Sciences, Guiyang 550002, China

ARTICLE INFO

Article history:
Received 3 April 2015
Received in revised form 26 September 2015
Accepted 26 September 2015
Available online 24 October 2015

Keywords:
Redox-stratified ocean
Euxinic condition
Oxidation mechanism
Ediacaran
Doushantuo Formation

ABSTRACT

Oceanic redox conditions and atmospheric oxygenation likely played a crucial role in the evolution of macroscopic multicellular eukaryotes during the early Ediacaran period. However, the oxidation mechanism and magnitude of the Ediacaran ocean–atmosphere system remain controversial. To constrain the oceanic redox conditions and the contemporaneous oxygenation of the atmosphere, we present a comprehensive investigation of redox-sensitive elements (e.g., Mo and U), Fe speciation and S isotopes of pyrite from the platform, slope and basin sections across the Doushantuo Formation in South China. Our results suggest a redox-stratified Ediacaran ocean with a fluctuating chemocline from the slope to platform location across the Doushantuo Formation. In particular, euxinic/intermittently euxinic conditions developed not only at the platform and slope but also in the deep basin. Furthermore, these euxinic conditions indicate that high sulfate concentrations may have accumulated not only at the ending of the Ediacaran Doushantuo Formation but also at the middle and beginning. Thus, these results suggest that the extensive euxinic conditions associated with the continuous oceanic sulfate input were in response to progressive oxygenation of the atmosphere during the early Ediacaran period. Integrated with previously published results, if the dissolved organic carbon (DOC) reservoir existed, different mechanisms may be responsible for the oxidation of deep ocean in each part of the studied sections across the Doushantuo Formation. One mechanism is oxidation by sulfate through a bacterial sulfate reduction (BSR) process under anoxic conditions. Another mechanism is oxidation by dissolved free oxygen under oxic/suboxic conditions. Finally, a dynamic evolution model of the Ediacaran ocean–atmosphere system across the Doushantuo Formation, South China, was suggested.

1. Introduction

The increasing oxygen levels and progressive oxygenation of the deep oceans throughout the entire Ediacaran (635–542 Ma) likely stimulated the radiation of macroscopic multicellular eukaryotes (Fike et al., 2006; Canfield et al., 2007; McFadden et al., 2008; Sahoo et al., 2012). Early animal evolution and diversification were commonly followed by an increased atmospheric oxygen concentration (e.g., Neoproterozoic Oxygenation Event) and a fluctuating marine environment. These have been intensively studied on the basis of multiple geochemical methods, such as carbon, sulfur, strontium, iron, chromium, uranium and molybdenum isotopes, redox-sensitive elements and iron speciation (Fike et al., 2006; Canfield et al., 2007, 2008; Jiang et al., 2007, 2011; Kaufman et al., 2007; Shields, 2007; McFadden et al., 2008; Scott et al., 2008; Shen et al., 2008; Frei et al., 2009; Li et al., 2010; Sahoo et al., 2012; Och and Shields-Zhou, 2012; Fan et al., 2014; Kendall et al., 2015). Although the mechanism and magnitude of the Neoproterozoic Oxygenation Event are still uncertain, a rise in atmospheric oxygen concentration has been widely recognized (Canfield and Teske, 1996; Canfield, 2005; Shen et al., 2008; Frei et al., 2009; Campbell and Squire, 2010; Sahoo et al., 2012; Och and Shields-Zhou, 2012). Nevertheless, the redox condition of the Ediacaran ocean remains open to debate and is the focus of conflicting viewpoints, such as whether there was an oxic or anoxic (ferruginous or euxinic) deep ocean. Several studies with investigations of Fe speciation, redox-sensitive elements and carbon, sulfur and nitrogen isotopes, have proposed that the Ediacaran deep ocean was widely oxygenated (Canfield, 1998; Fike et al., 2006; Canfield et al., 2007; Scott et al., 2008; Ader et al., 2014). However, other studies using similar geochemical approaches, have suggested a redox-stratified ocean (Jiang et al., 2007, 2011; Canfield et al., 2008; Shen et al., 2008; Ader et al., 2009; Li et al., 2010; Fan et al., 2014; Wood et al., 2015). Taking an example from the Ediacaran Doushantuo Formation in South China, alternative oceanic redox models have been proposed in recent years, such as the metastable zone of the euxinic water column sandwiched within anoxic open deep water at the platform and slope locations (Li et al., 2010; Wang

* Corresponding author.
E-mail address: fanhaifeng@mail.gyig.ac.cn (H. Fan).

http://dx.doi.org/10.1016/j.chemgeo.2015.09.021
0009-2541/

et al., 2012; Fan et al., 2014), or the strongly stratified shelf lagoon and open ocean with oxic shallow water and anoxic/euxinic deep water (Jiang et al., 2007, 2011).

The Ediacaran Doushantuo Formation, one of the best-preserved sedimentary sequences in the world, has been highly investigated in relation to its biological evolution, its stratigraphic correlation and the evolution of the ocean–atmosphere system (Xiao et al., 2002; Zhao et al., 2004; Zhou et al., 2007; McFadden et al., 2008; Xiao and Laflamme, 2008; Li et al., 2010; Jiang et al., 2011; Sahoo et al., 2012; Zhu et al., 2013). Fortunately, a number of integrated stratigraphy (including chemo- and chrono-) and paleogeography reviews have documented a wealth of fundamental information about the Doushantuo Formation (Zhou and Xiao, 2007; Zhu et al., 2007; Jiang et al., 2011; Xiao et al., 2012). Among the numerous geochemical efforts during the past decades, prominently negative carbonate carbon isotope ($\delta^{13}C_{carb}$) excursions have been characterized for the Doushantuo Formation in the Yangtze Three Gorges (Zhou and Xiao, 2007; Zhu et al., 2007; Jiang et al., 2007, 2011; McFadden et al., 2008). These were often correlated with other Ediacaran systems, such as those in Oman, Australia, Canada, Namibia, India, and the United States (Calver, 2000; Hoffman and Schrag, 2002; Jiang et al., 2002, 2003; Halverson et al., 2005; Fike et al., 2006; Kaufman et al., 2007; Le Guerroué and Cozzi, 2010). Several different hypotheses have been proposed for the origin of these unusually negative $\delta^{13}C_{carb}$ excursions, such as mantle-derived sources (Hoffman et al., 1998; Hoffman and Schrag, 2002), methane hydrate release (Kennedy et al., 2001; Jiang et al., 2003, 2006a; Bjerrum and Canfield, 2011), seawater overturn/upwelling (Kaufman et al., 1991; Knoll et al., 1996; Grotzinger and Knoll, 1995; Shields, 2005; Schröder and Grotzinger, 2007; Fan et al., 2014), and the oxidized weathering of terrigenous and marine organic-rich sediments (Kaufman et al., 2007; Higgins and Schrag, 2006). Additionally, another model has also been suggested which includes the oxidation of the deep oceanic dissolved organic carbon (DOC) reservoir (Rothman et al., 2003; Fike et al., 2006; Jiang et al., 2007; McFadden et al., 2008). If this DOC reservoir existed, the remineralization of deep oceanic DOC was likely related to the oxygenation of the Ediacaran ocean–atmosphere system (Fike et al., 2006; Jiang et al., 2007; McFadden et al., 2008; Fan et al., 2014). Furthermore, S isotopes, Fe speciation and redox-sensitive elements have also been used to reconstruct the paleoceanographic environment of the Ediacaran Doushantuo Formation. Despite the lower-resolution samples and the lack of comparison among different sedimentary sections, these geochemical data have still provided relevant information for continued investigation of the ocean redox conditions and atmospheric oxygenation in the Ediacaran (McFadden et al., 2008; Shen et al., 2008; Li et al., 2010; Sahoo et al., 2012).

To constrain the oceanic redox conditions and the atmospheric oxygenation during the Ediacaran Doushantuo period, the high resolution variations in redox-sensitive elements (e.g., Mo and U) coupled with Fe speciation and S isotope data of the comprehensive sedimentary facies including platform, slope and basin sections, all from the Doushantuo Formation, were investigated in this contribution. Based on our data in combination with previously published results, we would like to suggest a dynamic evolution model of the Ediacaran ocean–atmosphere system across the Doushantuo Formation, South China.

2. Geological backgrounds

The Ediacaran Doushantuo Formation, which constrained between 635.2 ± 0.6 Ma and 551.1 ± 0.7 Ma by zircon U–Pb ages of interbedded volcanic ash, is underlain closely by the Cryogenian Nantuo Formation and is deposited at a passive continental margin setting, without tectonic events and igneous activities, in South China (Fig. 1; Condon et al., 2005; Jiang et al., 2011). The sediment of the Doushantuo Formation commonly starts with the cap carbonate and terminates with organic-rich black shale. Whether on the platform or in the slope and basin facies, the similar lithology and geochemical characteristics of the cap carbonate make it a lithostratigraphic marker bed at the base of the Doushantuo Formation (Jiang et al., 2006b, 2011). After the cap carbonate, the sedimentary facies and the thickness of the Doushantuo Formation exhibit large variations from the platform, to the slope to the basin (Zhu et al., 2007; Jiang et al., 2011; Wang, 2012). In general, the platform section is dominated by interbedded carbonate and black shale, whereas the main lithology of black shale is characterized for the slope and basin locations (Zhu et al., 2007; Jiang et al., 2011; Wang, 2012). At the top of the Doushantuo Formation, the organic-rich black shale is recommended as another regional lithostratigraphic marker bed because it can distinguish the Doushantuo Formation from the overlying Dengying/Liuchapo/Laobao Formations (Jiang et al., 2011; Wang, 2012).

In this work, two well-studied sections (the platform, Jiulongwan, and the slope, Wuhe) and one new basin section (Xiangtan) are included and provide a comprehensive comparison across the Doushantuo Formation (Fig. 1). The Jiulongwan section, one of the most well-known sections, is located in the Yangtze Gorges area with a rough thickness of 155 m, and it can be divided into four members as follows. Member 1 consists of cap carbonate with a thickness of approximately 5 m at the base of the Doushantuo Formation. Member 2 (ca. 80 m) contains interbedded carbonates and organic-rich black shale accompanied by numerous pea-sized chert nodules. Member 3 (ca. 60 m) is primarily characterized by carbonates with bedded chert layers and minor shale beds. Member 4 (ca. 10 m) is mainly deposited as the organic-rich black shale at the top of the Doushantuo Formation (Fig. 2; McFadden et al., 2008; Li et al., 2010; Jiang et al., 2011; Wang, 2012).

Nevertheless, these distinctive features and divisions in the Jiulongwan platform section are not identified in the Wuhe slope and Xiangtan basin sections due to the absence of correlation of the biostratigraphy and lithostratigraphy. Therefore, the variations of geochemical lines are expected to provide rough evolutionary stages in this study. The Doushantuo Formation in the Wuhe section, with a thickness of approximately 120 m, has approximately 2.5 m of cap carbonate and 5 m of organic-rich black shale, which are distributed at the base and top of the Doushantuo Formation, respectively. The remainder of the Wuhe section is mainly characterized by interbedded black shale and carbonates, with a few olistostrome layers (Fig. 3; Jiang et al., 2007; Sahoo et al., 2012; Wang, 2012). Regarding the Xiangtan basin section, the overall thickness of the Doushantuo Formation is approximately 190 m, and black shale is the predominated feature. The distinctive markers of the Doushantuo Formation in the Xiangtan section, distinguishing it from the underlying Nantuo Formation and the overlying Liuchapo Formation, are mainly based on the distributions of the underlying cap carbonate and the overlying chert layer (Fig. 4).

3. Samples and methods

3.1. Samples

All of the studied black shale samples were freshly collected from the Jiulongwan (30°48′54″N, 110°3′20″E, 36 samples, platform, Fig. 2), Wuhe (26°45′57″N, 108°24′59″E, 48 samples, slope, Fig. 3) and Xiangtan (27°58′24″N, 112°49′51″E, drill-hole samples, 52 samples, basin, Fig. 4) sections. These samples were ground to minus 200 mesh in an agate mortar for further elemental analysis. The Fe speciation and S isotope of the Jiulongwan section were cited from Li et al. (2010) and McFadden et al. (2008). Another data of Mo, U and Fe speciation of the upper part of the Jiulongwan section (Member 4) were cited from Kendall et al. (2015) (Fig. 2). In addition, other further 25 data points for black shale samples from the base (21 samples from 2.4–8.6 m) and the top (4 samples from 117 to 120 m) of the Wuhe section were taken from Sahoo et al. (2012) and Wang (2012), respectively (Electronic Appendix Table 1).

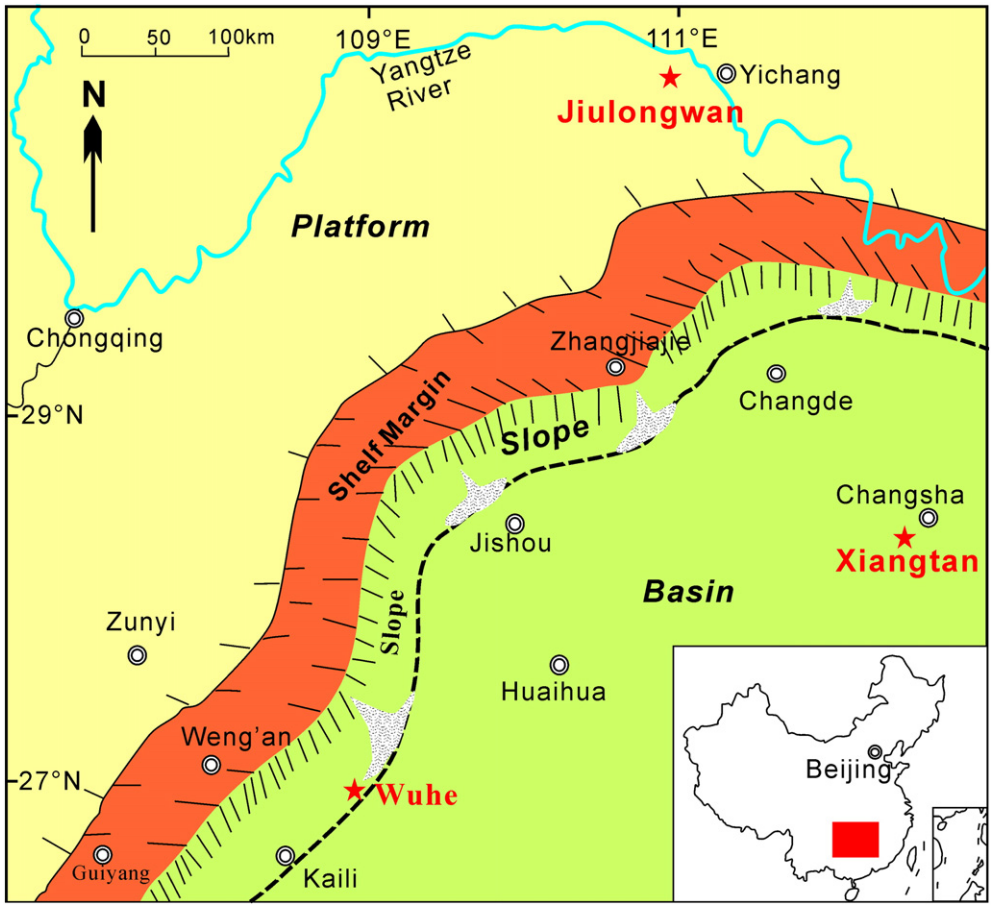

Fig. 1. Paleogeographic reconstruction of the Ediacaran Doushantuo Formation in South China (modified after Jiang et al., 2011; Guo et al., 2011), the five-pointed star symbols are the locations of the studied sections.

3.2. Analytical methods

The concentrations of Mo and U in black shale samples were determined by a Perkin-Elmer Sciex ELAN DRC-e ICP-MS at the State Key Laboratory of Ore Deposit Geochemistry (SKLODG), Institute of Geochemistry, Chinese Academy of Sciences. A 50 mg powder sample was dissolved in a high-pressure Teflon bomb with HF and HNO_3 at 190 °C for 48 h. Subsequently, the residue was redissolved in H_2O and HNO_3 with an appropriate amount of Rh at 145 °C for 12 h. The Rh was used as an internal standard to monitor instrumental drift during

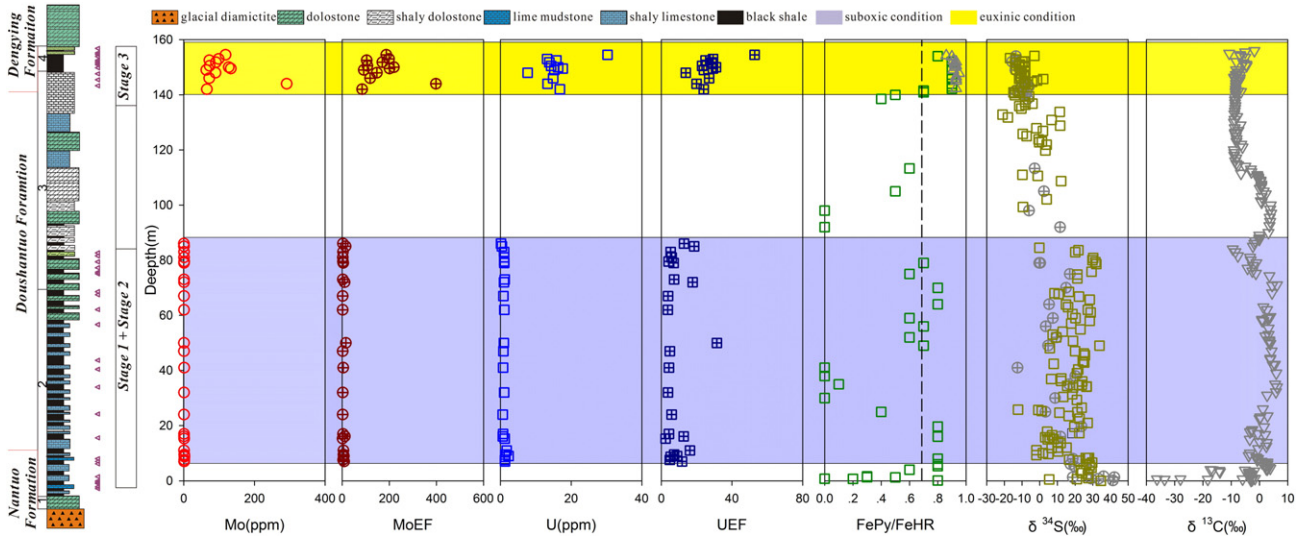

Fig. 2. Lithological column (modified after Jiang et al., 2011), sampling locations, authigenic Mo–U enrichment and other collected published geochemical data of the Jiulongwan platform section. Data of the $\delta^{34}S_{pyrite}$ are from McFadden et al. (2008) (square) and Li et al. (2010) (rotundity); data of Fe_{py}/Fe_{HR} are from Li et al. (2010) (square) and Kendall et al. (2015) (triangle) with a dashed line $Fe_{py}/Fe_{HR} = 0.7$ (Poulton and Canfield, 2011 and references therein) and data of $\delta^{13}C_{carb}$ are from Jiang et al. (2007).

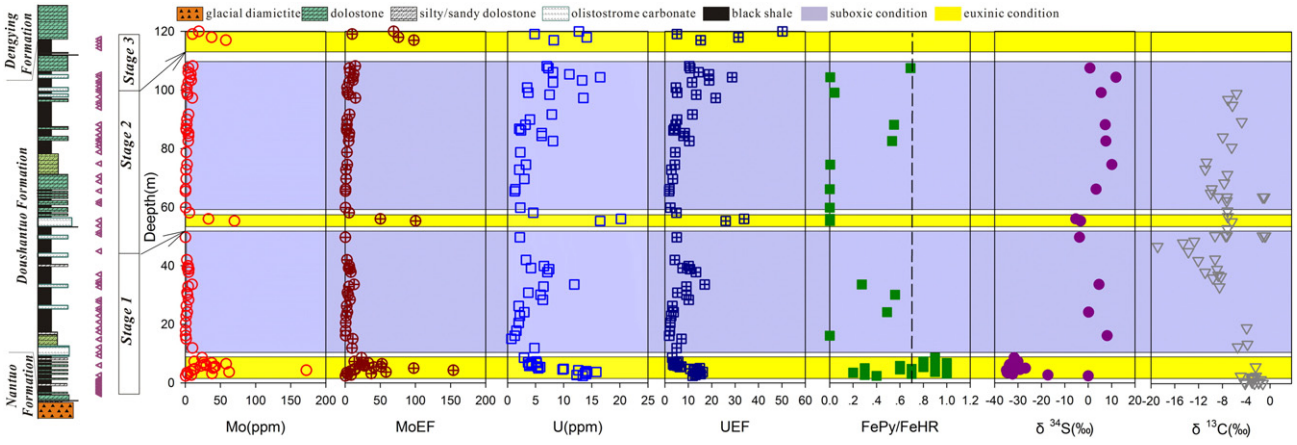

Fig. 3. Lithological column (modified after Jiang et al., 2011), sampling locations, authigenic Mo–U enrichment and other collected published geochemical data of the Wuhe slope section. Data of the lower enriched part (21 samples from 2.4–8.6 m) and the upper enriched part (4 samples from 117 to 120 m) of the Wuhe section are collected from Sahoo et al. (2012) and Wang (2012), respectively; data of $\delta^{13}C_{carb}$ are from Jiang et al. (2007). Dashed line with $Fe_{py}/Fe_{HR} = 0.7$ for distinguishing euxinic from ferruginous water columns (Poulton and Canfield, 2011 and references therein).

the analysis (Qi et al., 2000). The standard reference materials AGV-2, AMH and GBPG were measured together with our samples (Electronic Appendix Table 1). Al and Fe concentrations were determined by a PANalytical B.V. Axios (PW4400) X-ray fluorescence spectrometer (XRF) at the SKLODG, Institute of Geochemistry, Chinese Academy of Sciences. A 0.7 g sample and 7 g of composite flux ($Li_2B_4O_7 + LiBO_2 + LiF$) was melted at 1100 °C into fused glass disks for determination, and the Chinese standard reference material (GSR-5: black shale) was analyzed together (Electronic Appendix Table 1). Total S contents were measured by a Leco CS230 carbon and sulfur analyzer at the ALS Chemex (Guangzhou) Company Limited and the relative standard deviation was better than 5%.

Analyses of Fe speciation and S isotopes of pyrite were carried out at the State Key Laboratory of Biogeology and Environmental Geology, China University of Geosciences (Wuhan) according to a previously published procedure (Li et al., 2010). The highly reactive iron (Fe_{HR}) consists of pyrite (Fe_{py}), carbonate-associated iron (Fe_{carb}), ferric oxides (Fe_{ox}) and magnetite (Fe_{mag}). Fe_{carb}, Fe_{ox} and Fe_{mag} concentrations were extracted sequentially by sodium acetate solution, sodium dithionite solution and ammonium oxalate and then determined by ICPMS. Fe_{py} was calculated from the sulfur concentration of pyrite determined by the chromium reduction method. The precision of Fe speciation data was monitored by duplicate samples. The S isotope composition was reported as per mil deviations from the V-CDT international standard, and the results of standard reference materials for IAEA S1, IAEA S2 and IAEA S3 were −0.2‰, 22.7‰ and −32.3‰, respectively.

An enrichment factor (EF), as used in previous studies, was applied to describe the authigenic Mo–U enrichment with the equation $X_{EF} = [(X/Al)_{sample}/(X/Al)_{PAAS}]$ (Tribovillard et al., 2006, 2012; Algeo and Tribovillard, 2009). The values of X and Al refer to their weight concentrations, and the PAAS (post-Archean average shale) data for normalization were from Taylor and Mclennan (1985). In addition, although the

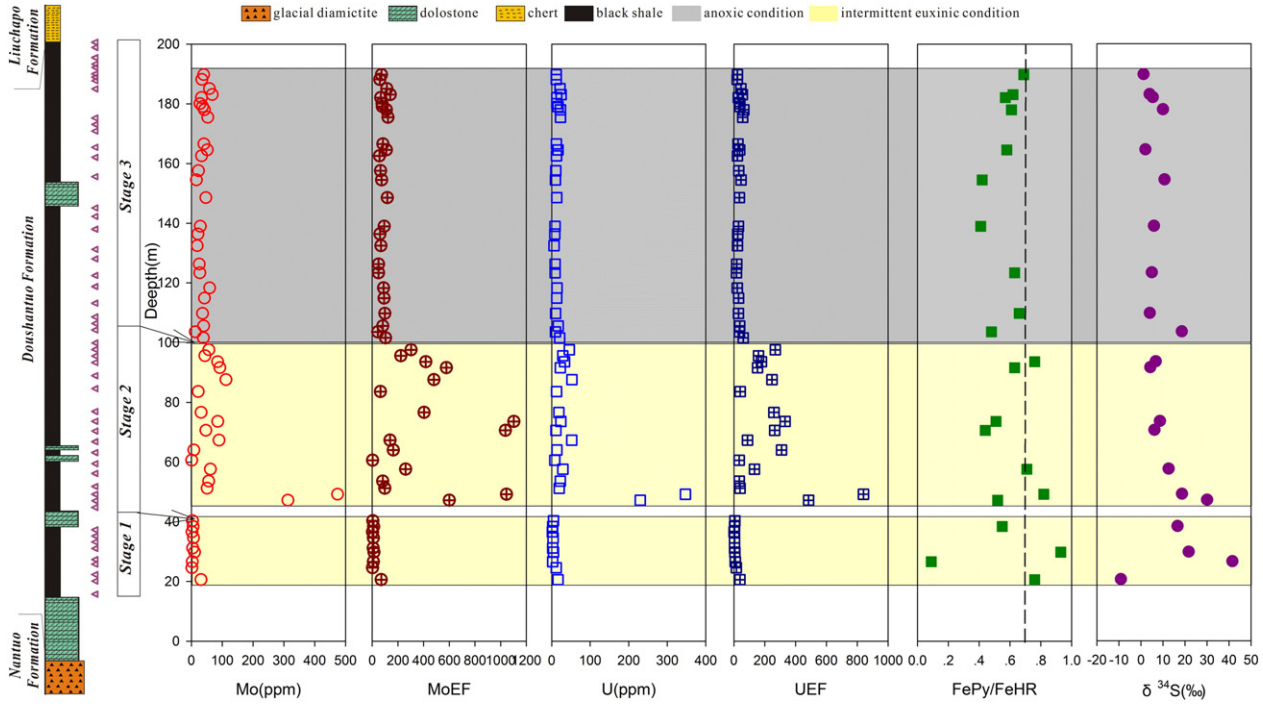

Fig. 4. Lithological column, sampling locations, authigenic Mo–U enrichment of the basin Xiangtan section. Dashed line with $Fe_{py}/Fe_{HR} = 0.7$ for distinguishing euxinic from ferruginous water columns (Poulton and Canfield, 2011 and references therein).

concentrations of Mo and U during the Ediacaran seawater are uncertain, the $(Mo/U)_{auth}$ ratio (average modern seawater weight ratio is about 3.1 and molar ratio is 7.5 to 7.9, Tribovillard et al., 2012), was used here to compare the relative degree of authigenic Mo–U enrichment among the studied sections during the Doushantuo Formation. Note that the application of the redox-sensitive elements for sedimentary analyses must be consistent with their exclusive seawater uptake, rather than the detrital origin. In general, the correlation coefficient between the given element and Al or Ti can confirm whether the given element is controlled by the detrital flux (Tribovillard et al., 1994, 2006). In our studied sections, an absence of positive correlations was observed among Mo, U and Al (Fig. 5), which indicates that Mo and U were not affected by the detrital components and can be used as proxies for paleo-environmental investigation of the Doushantuo Formation.

4. Results

All of the data are listed in the Electronic Appendix Table 1. Three different distributions shown in the Doushantuo Formation based on the above-mentioned geochemical parameters, and they are referred to as the lower part, the middle part and the upper part, with an approximate relative location for each section in this study (Figs. 2, 3 and 4).

4.1. Jiulongwan platform section

In the lower part (7–86 m) of the Jiulongwan section, the concentrations of Mo and U were equal to or less than the crustal values in most samples, with values ranging from 0.0 to 2.0 ppm and 0.1 to 2.3 ppm, respectively (Fig. 2). This part also has low EFs ranging from 1.6 to 15.7 for

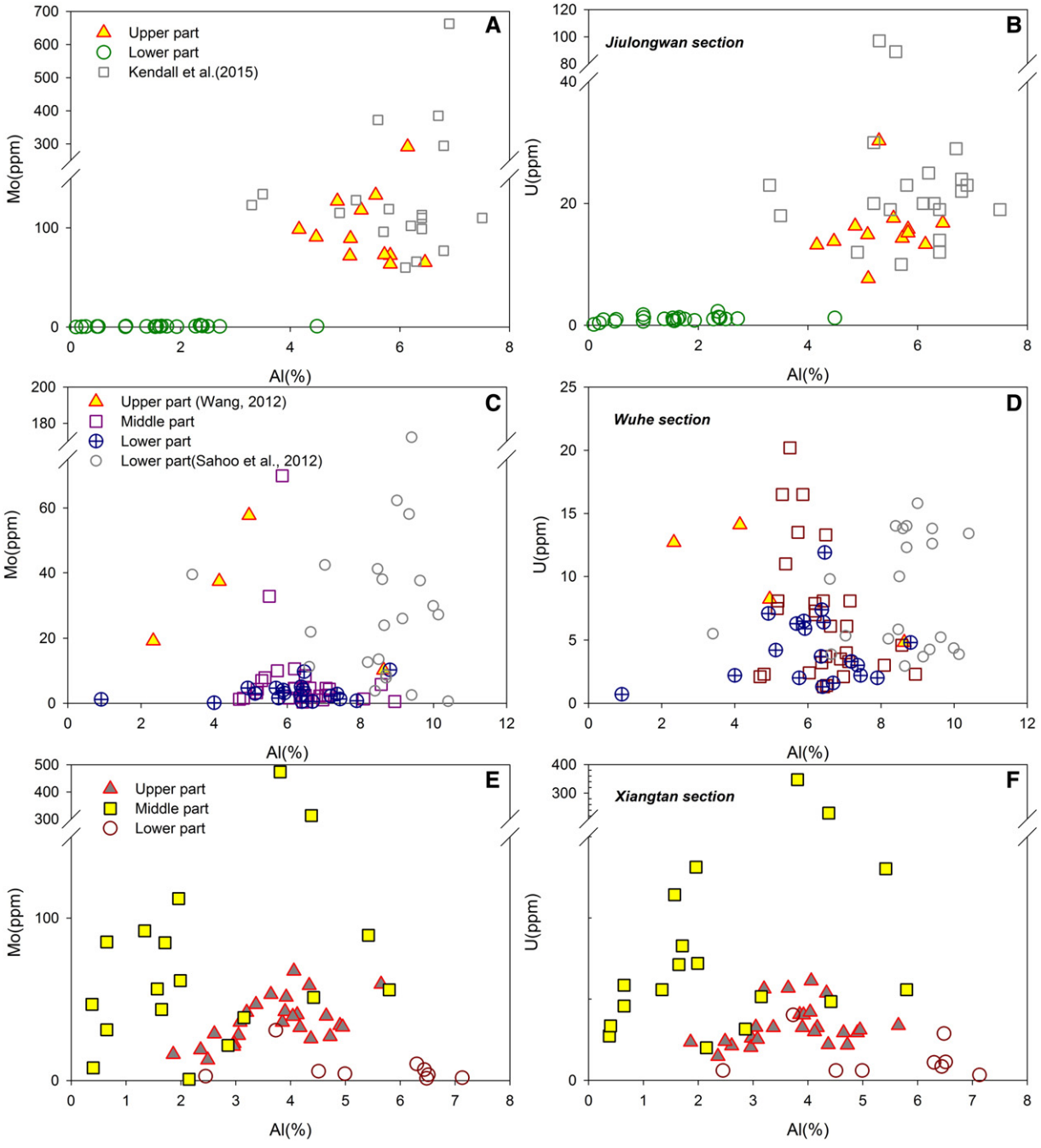

Fig. 5. Scatter diagram among Mo, U and Al of the black shale samples in the studied sections for checking whether the given element is controlled by the detrital flux.

Mo and 2.5 to 31.5 for U, and it has low $(Mo/U)_{auth}$ ratios less than 0.3 times that of modern seawater in most samples. The sulfur isotope ratios of pyrite ($\delta^{34}S_{pyrite}$) in this lower part varied substantially and ranged from −12.6 to 33.8‰. Moreover, Fe_{py}/Fe_{HR} ratios of the lower part also changed substantially and ranged from 0 to 0.8 (Li et al., 2010; Kendall et al., 2015; Fig. 2).

In contrast, Mo and U were strongly enriched in the upper part (142–155 m) of the Jiulongwan section, with sharp increases from 63.6 to 291.0 ppm for Mo and from 7.7 to 30.3 ppm for U (Fig. 2). These elemental distributions also corresponded to high EFs ranging from 84.8 to 398.0 for Mo and 13.9 to 52.8 for U (Fig. 2). Additionally, the strongly enriched upper part mainly exhibited $(Mo/U)_{auth}$ ratios between one and six times that of modern seawater (Fig. 6). In addition, the upper part of the Jiulongwan section exhibited negative $\delta^{34}S_{pyrite}$ values ranging from −3.0 to −16.8‰. The Fe_{py}/Fe_{HR} ratios of the upper part had relatively uniform values near 0.9 (Li et al., 2010; Kendall et al., 2015; Fig. 2).

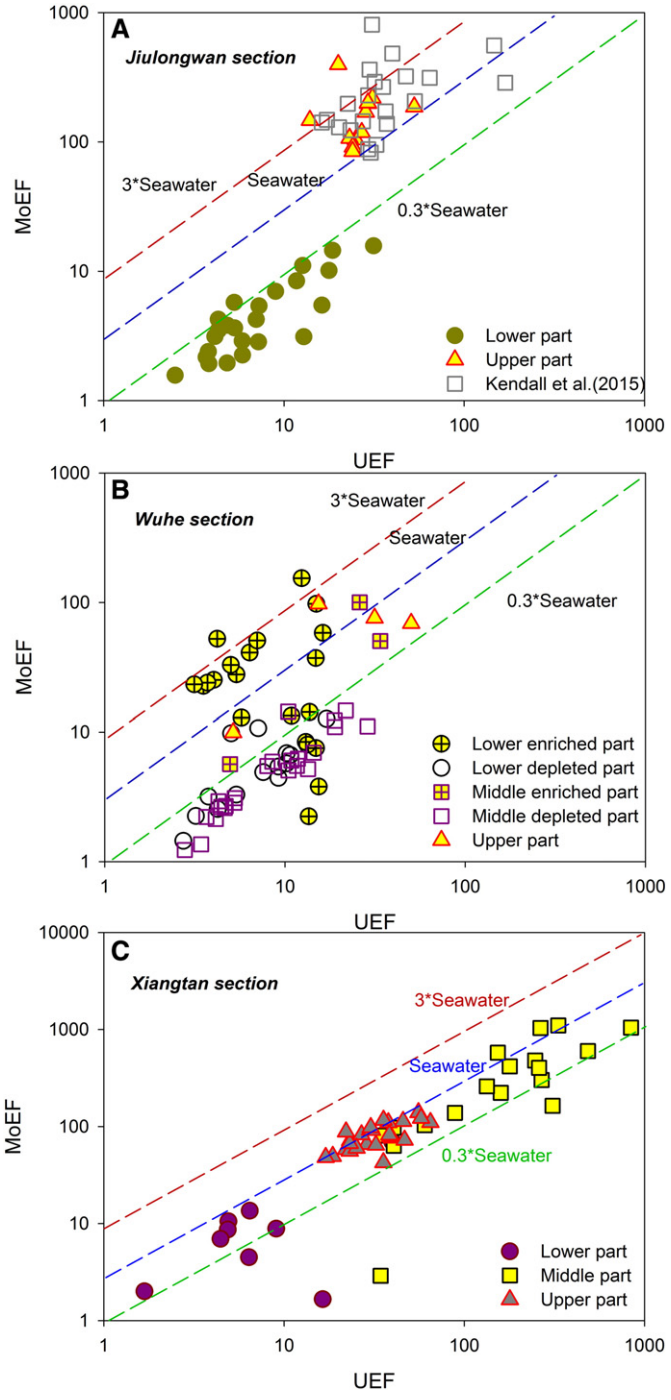

Fig. 6. $(Mo/U)_{auth}$ ratios of the black shale samples in the studied sections for the degree of enrichment between the authigenic Mo and U, the average Mo/U weight ratio of seawater is 3.1 (the Mo/U molar ratio is 7.5–7.9, Algeo and Tribovillard, 2009; Tribovillard et al., 2012). Data of Mo and U (square) of upper part (Member 4) in the Jiulongwan section are from Kendall et al. (2015) and data of the lower enriched part and the upper part of the Wuhe section are collected from Sahoo et al. (2012) and Wang (2012), respectively.

4.2. Wuhe slope section

Three distinctive enriched intervals for Mo and U were observed in the lower, middle, and upper parts of the Wuhe slope section, with rough locations at 2.4–8.6 m (lower enriched part), 55.3–56 m (middle enriched part) and 117–120 m (upper part), respectively (Fig. 3). Nevertheless, the remainder of the samples (e.g., lower depleted and middle depleted parts) typically showed relatively low Mo concentrations ranging from 0.1 ppm to 10.6 ppm, and low EFs ranging from 0.3 to 14.6 (Fig. 3). In terms of the three enriched intervals, most samples had high Mo concentrations (tens of ppm) and EFs, and one sample reached 172 ppm with EFs of 154 (Fig. 3). In contrast, throughout the black shale sample of the Wuhe section, the concentrations of U did not vary markedly, with values ranging from 0.7 ppm to 20.2 ppm. Moreover, the EFs of U for most samples were typically less than 20, except for a few samples with EFs between 20 and 50 (Fig. 3). Above all, most samples of the three enriched intervals (lower enriched, middle enriched and upper parts) had $(Mo/U)_{auth}$ ratios between 0.3 and four times that of modern seawater, and these were much higher than those of the lower depleted and middle depleted parts, which are equal to or less than 0.3 times that of modern seawater (Fig. 6).

Moreover, the $\delta^{34}S_{pyrite}$ values of the lower enriched part and middle enriched parts were similar to those of the upper part of the Jiulongwan section and ranged from −17.2 to −34.6‰ and −3.2 to −5.3‰, respectively (Sahoo et al., 2012; Fig. 3). These highly negative $\delta^{34}S_{pyrite}$ values were different from those of the lower depleted and middle depleted samples with values ranging from 0.2 to 8.1‰ and 0.8 to 11.9‰, respectively (Fig. 3). However, the distributions of the Fe_{py}/Fe_{HR} ratios for the lower enriched part and middle enriched parts are inconsistent, such as 0.20–1 for the lower enriched part and 0 for the middle enriched part. Furthermore, the Fe_{py}/Fe_{HR} ratios of the lower depleted and middle depleted parts were irregular and ranged from 0 to 0.69 (Fig. 3). Unfortunately, we failed to collect the samples and obtain the Fe speciation and S isotope data for the upper part in the Wuhe section.

4.3. Xiangtan basin section

The Xiangtan section showed strongly authigenic Mo–U enrichment compared with the Jiulongwan and Wuhe sections. Most black shale samples of the Xiangtan section were characterized by high Mo and U concentrations and EFs. There were also three different distributions observed in the Xiangtan basin section. For the lower part (20.6–40.3 m), the concentrations ranged from 1.3 to 30.9 ppm with EFs between 1.7 and 69.6 for Mo, and from 1.3 to 16.1 ppm with EFs between 1.7 and 39.8 for U (Fig. 4). Subsequently, abruptly increasing and largely fluctuating authigenic Mo–U enrichments were found in the middle part of this basin section (47.2–102 m). The concentrations of Mo ranged from 0.7 to 474 ppm with EFs between 2.9 and 1102. Similarly, the concentrations of U ranged from 8.0 to 347.0 ppm, with EFs between 34.5 and 841 in the middle of the Xiangtan section (Fig. 4). It appeared that a relatively stable elemental enrichment was present in the upper part of the Xiangtan section (104–190 m), where the concentrations ranged from 12.7 to 67.4 ppm with EFs between 42.7 and 139.0 for Mo, and from 5.9 to 24.5 ppm with EFs between 17.0 and 64.9 for U (Fig. 4). In

particular, with respect to the $(Mo/U)_{auth}$ ratios, almost all of the samples were between 0.3 and one times that of modern seawater (Fig. 6).

The $\delta^{34}S_{pyrite}$ results of the lower, middle and upper parts for the Xiangtan section were within the scope of −9.1–41.6‰, 4.2–30.0‰ and 1.17–18.5‰, respectively (Fig. 4). Furthermore, the Fe_{py}/Fe_{HR} ratios ranged from 0.09 to 0.93 and 0.44 to 0.82 in the lower and middle parts, which were slightly higher than those of the upper part (0.41 to 0.69) (Fig. 4).

5. Discussion

5.1. The principle of the multiple paleo-redox proxies

The geochemical behavior of the redox-sensitive elements Mo and U have been intensively investigated and understood in seawater, which could make them useful for reconstructing and evaluating the marine paleo-environment reliably and effectively (Anderson et al., 1989; Klinkhammer and Palmer, 1991; Crusius et al., 1996; Helz et al., 1996; Erickson and Helz, 2000; Zheng et al., 2000; Chaillou et al., 2002; Vorlicek and Helz, 2002; Tribovillard et al., 2004; Vorlicek et al., 2004; Algeo and Maynard, 2004). The differences among the geochemical characteristics of Mo and U regulate their distributions and facilitate their different behaviors under oxic and anoxic (ferruginous or euxinic) conditions. In one situation, Mo is primarily sensitive to the extent of euxinic conditions and can be strongly enriched in anoxic conditions in the presence of free hydrogen sulfide (H_2S) (Scott et al., 2008; Sahoo et al., 2012; Scott and Lyons, 2012). This enrichment is usually achieved by the conversion of soluble MoO_4^{2-} to particle-reactive thiomolybdates ($MoO_xS_{4-x}^{2-}$, x = 0–3) which can subsequently be effectively captured by metal-rich particles or sulfidized organic materials (Helz et al., 1996; Erickson and Helz, 2000; Tribovillard et al., 2004; Vorlicek et al., 2004). On the other side, U is more sensitive than Mo to the extent of suboxic and ferruginous conditions and the enrichment of U commences under suboxic condition, near the redox interface between Fe (III) and Fe (II), via the formation of UO_2, U_3O_7, or U_3O_8 in sediment (Klinkhammer and Palmer, 1991; Crusius et al., 1996; Zheng et al., 2000; Chaillou et al., 2002; Partin et al., 2013).

Previous studies have proposed several geochemical indicators (e.g., EF, $(Mo/U)_{auth}$ ratio, and Mo concentration) based on Mo and U relationships in the modern marine system that have also been applied to the study of paleoceanography (Tribovillard et al., 2006, 2012; Algeo and Tribovillard, 2009; Scott and Lyons, 2012). Here, and first, the concentrations of Mo and U under oxic conditions were very low and close to those of the upper continental crust. Second, under suboxic conditions, authigenic U enrichment tended to be higher than that of Mo, with the EFs often less than 10, and the $(Mo/U)_{auth}$ ratios were equal to or less than 0.3 times that of modern seawater. Third, under anoxic to euxinic conditions, the authigenic Mo enrichment exceeded that of U, with the EFs being more than 10, and the $(Mo/U)_{auth}$ ratios approaching, or even exceeding that of modern seawater (Algeo and Tribovillard, 2009; Tribovillard et al., 2012). Furthermore, the concentration of Mo can also provide indications of paleo-redox conditions as follows. For instance, Mo enrichment between the crustal value and 25 ppm indicates non-euxinic condition with dissolved H_2S restricted to the pore water; whereas Mo enrichment exceeding 100 ppm shows permanently euxinic condition, and Mo enrichment between 25 and 100 ppm can result from other complicated factors, but it at least indicates the occurrence of intermittently euxinic bottom waters (Scott and Lyons, 2012). Nevertheless, the concentrations of Mo and U during the Ediacaran seawater are uncertain, the $(Mo/U)_{auth}$ ratio used here could show the relative degree of authigenic Mo–U enrichment among the studied sections.

The analysis of Fe speciation has been applied to large amount studies of paleo-ocean redox conditions (e.g., Canfield et al., 2008; Li et al., 2010; Sahoo et al., 2012). The main principle of this methodology is to obtain total Fe content and highly reactive mineral Fe species (e.g., pyrite, Fe oxides, magnetite and carbonate-associated species). Many previous studies have concluded that Fe_{HR}/Fe_T ratios greater than 0.38 or 0.15 (if suffered by metamorphism) indicate anoxic conditions, whereas Fe_{py}/Fe_{HR} ratios greater than 0.7 point to euxinic conditions (Raiswell et al., 2008; Poulton and Canfield, 2011 and references therein). However, Sahoo et al. (2012) suggested that the Fe_{HR}/Fe_T ratio may be not suitable to delineate anoxia because the unusually low Fe/Al ratios were not well understood, but the Fe_{py}/Fe_{HR} ratio can be used to distinguish the euxinic (sulfidic) from ferruginous (nonsulfidic) water column during the Doushantuo Formation.

5.2. The redox conditions of three studied sections across the Doushantuo Formation

5.2.1. Jiulongwan platform section

In the Jiulongwan platform section, the authigenic Mo–U enrichment, Fe speciation and S isotope ratios of the black shale samples exhibit a clear trend from suboxic to euxinic conditions.

For the lower part, unambiguous features in most samples, such as the similar crustal concentrations, low EFs (~10), and low $(Mo/U)_{auth}$ ratios (~0.3 times that of modern seawater), were consistent with those of suboxic conditions (Figs. 2 and 6). Nevertheless, the suboxic conditions of the lower part inferred here was incompatible with the previous two euxinic episodes indicated by the Fe speciation study (Li et al., 2010). This contradiction might be caused by the formation of pyrite during the diagenetic process, and the explanation can be inferred by the S isotope ratios and total S contents. The $\delta^{34}S_{pyrite}$, with values generally between 20‰ and 30‰, and relatively small S isotope fractionation between pyrite and sulfate in most samples (McFadden et al., 2008; Li et al., 2010, Fig. 2) appear to indicate that BSR processes are impossible in this environment. In addition, the extremely low and variable total S content (0.03 to 1.93%, Electronic Appendix Table 1) should not be compatible with anoxic conditions where the S is buried steadily, but it should be consistent with suboxic conditions where the S was easy to activate and lose. Hence, together with the absence of enrichment of Mo and U, the suboxic conditions might be much more reasonable in the lower part of the Jiulongwan section. In another aspect, high $\delta^{238}U$, low $\delta^{98}Mo$ and high Mo concentrations in the upper part suggest a large seawater Mo inventory in well-oxygenated oceans (Kendall et al., 2015), which seems consistent with the indication of prevailing suboxic conditions before the deposition of the upper part.

Furthermore, high concentrations (up to 291.0 ppm Mo and 30.3 ppm U), high EFs (up to 398.0 for Mo and 52.8 for U) and high $(Mo/U)_{auth}$ ratios (1–6 times that of modern seawater) in the black shale samples of the upper part (Figs. 2 and 6) indicated that these strongly authigenic Mo–U enrichments occurred under euxinic conditions in the presence of free H_2S. Moreover, the euxinic conditions in the upper part of this study area were compatible with the previous indications of Fe speciation (Li et al., 2010; Kendall et al., 2015). This consistency can also be supported by the negative $\delta^{34}S_{pyrite}$ values and large S isotope fractionation, which may result from the BSR processes (McFadden et al., 2008; Li et al., 2010). Moreover, the total S content of the upper part (2.38 to 3.70%) was higher than that of the lower part (0.03 to 1.93%), which also suggests different sedimentary conditions for the lower and upper parts (Electronic Appendix Table 1).

5.2.2. Wuhe slope section

The redox condition at the Wuhe slope section varied repeatedly between euxinic and suboxic conditions during the sedimentary period of the lower, middle and upper parts. This situation may be attributed to the fluctuating chemocline.

In most samples from the lower and middle enriched parts, the Mo concentrations were between 25 and 100 ppm, EFs were much greater than 10, and $(Mo/U)_{auth}$ ratios were between one and four times that of modern seawater (Figs. 3, 6). All of these Mo–U features indicated that two euxinic episodes may have occurred during the early sedimentary

period of the Wuhe section. The Fe_{py}/Fe_{HR} ratios of most samples in the lower enriched part were exceeding 0.7, which indicates the occurrence of euxinic conditions (Sahoo et al., 2012). Furthermore, negative $\delta^{34}S_{pyrite}$ values and large S isotope fractionation of the lower enriched part were compatible with BSR processes, which was similar to the upper part of the Jiulongwan section. However, the Fe_{py}/Fe_{HR} ratios of the middle enriched part near zero ($Fe_{py}/Fe_{HR} = 0$) were not compatible with the euxinic conditions inferred from authigenic Mo–U enrichment. The negative $\delta^{34}S_{pyrite}$ values with large S isotope fractionation of the middle part are similar to the characteristics of the upper part of the Jiulongwan section, which indicated the presence of BSR process. These extremely low Fe_{py}/Fe_{HR} ratios might have resulted from the re-oxidation of buried pyrite under the suboxic conditions that occurred later. Hence, there are two transient euxinic conditions that may be have ever occurred in the lower and middle parts. In contrast, minor concentrations, low EFs and modest enrichment of U (relative to Mo) in most of the samples of the lower depleted and middle depleted parts suggested that suboxic conditions dominated during the sedimentation of the Wuhe slope section. This presence of suboxic conditions was compatible with the irregular Fe_{py}/Fe_{HR} ratios (0–0.69), the $\delta^{34}S_{pyrite}$ values (0.2–11.9‰), and the low or variable total S content (0.01–3.62%) (Fig. 3, Electronic Appendix Table 1). In regard to the upper part, despite the absence of S isotope and Fe speciation data, the modest enrichment of Mo and U coupled with the pyrite morphology study (Wang et al., 2012) suggest the presence of a euxinic water column in the upper part of the Wuhe section. That is to say, three euxinic conditions occurred transiently during the prevailing suboxic condition because of the fluctuating chemocline throughout the Doushantuo Formation.

In brief, these studies suggest that the euxinic conditions may have occurred not only in the shallow platform (Jiulongwan section) but also in the slope location (Wuhe section).

5.2.3. Xiangtan basin section

Compared with the Jiulongwan and Wuhe sections, the Xiangtan basin section exhibited large authigenic Mo–U enrichment and variable Fe_{py}/Fe_{HR} ratios and S isotope values, which indicated fluctuating oceanic chemical conditions and prevalent anoxic/intermittent euxinic conditions during the sedimentary period.

Three distinctive oceanic conditions occurring during the sedimentary period of the Xiangtan section can be identified. In the lower part, the concentrations and EFs in most samples were less than 10, but were higher than the crustal value and those of the suboxic samples in the Jiulongwan and Wuhe sections. Moreover, the $(Mo/U)_{auth}$ ratios varied substantially (0–0.7 times that of modern seawater) and were also inconsistent with the suboxic portions of the Jiulongwan and Wuhe sections (less than 0.3 times that of modern seawater) (Figs. 4, 6). This enrichment pattern could be explained by the occasional occurrence of H_2S under anoxic conditions. Additionally, high Fe_{py}/Fe_{HR} ratios greater than 0.7 in a few black shale samples also indicated that an intermittently euxinic water column occurred in the lower part. Subsequently, the middle part contributed fluctuating concentrations, EFs, and $(Mo/U)_{auth}$ ratios (0–1 times that of modern seawater). In the same way, a few samples in the middle part with Fe_{py}/Fe_{HR} ratios that are greater than 0.7 suggested the occurrence of an intermittently euxinic water column under anoxic conditions in the middle part (Fig. 4). Finally, the modest authigenic Mo–U enrichment, Fe_{py}/Fe_{HR} ratios less than 0.7 and modest S isotope fractionation suggested anoxic conditions in the upper part of the Xiangtan section). Additionally, this anoxic condition might be ferruginous, which could be indicated by the ratio of total Fe to S (Fe/S ratio). The Fe/S ratios of the upper part in the Xiangtan section (0.83–1.71) are higher than that of stoichiometric pyrite (Fe/S = 0.875) and those of the upper part of the Jiulongwan section (0.68–1.02) (Electronic Appendix Table 1).

In summary, an intermittently euxinic water column occurred in the lower and middle parts of the Xiangtan section, but an episode of anoxic ferruginous conditions occurred in the upper part. Furthermore, at another basin section (Yuanjia Hu'nan Province), the lower part closely followed the cap carbonate in showing significant authigenic Mo and U enrichment and high Fe_{py}/Fe_{HR} values greater than 0.7, which indicated a potentially euxinic water column (Sahoo et al., 2012). Thus, these studies revealed that euxinic conditions have occurred not only in the platform and slope locations but also in the deep basin.

5.3. Evolution of the Ediacaran ocean–atmosphere system

5.3.1. A possible link among these multiple geochemical data

The wide variety of C and S isotopes, Fe speciation and redox-sensitive element studies are the most useful tools for understanding the Ediacaran ocean–atmosphere system (Hurtgen et al., 2005; Fike et al., 2006; Canfield et al., 2000, 2007, 2008; Halverson and Hurtgen, 2007; McFadden et al., 2008; Shen et al., 2008; Jiang et al., 2011). However, the detailed relationships among oceanic redox condition, atmospheric oxygenation, and these geochemical data remain unclear. In this study, using our results and previously published data across the Doushantuo Formation, we attempt to explore a possible link among them.

S isotopes have been used intensively for studying the evolution of atmospheric oxygen because oceanic sulfate accumulation is closely influenced by the atmospheric oxidative weathering of sulfides on land (Canfield et al., 2000). In addition, the bacterial sulfate reduction (BSR) processes below the chemocline played an important role in S isotope fractionation ($\Delta^{34}S_{sulfate-pyrite}$: isotope fractionation between sulfate and pyrite), where the sulfate is enriched in ^{34}S and sulfide is depleted in ^{34}S (Canfield and Thamdrup, 1994). Previous experimental studies have demonstrated that, with sufficient sulfate (>200 μM), the BSR processes could produce a large degree of S isotope fractionation (up to 70‰) in marine sediments (Habicht and Canfield, 2001; Habicht et al., 2002; Canfield et al., 2010). Across the Doushantuo Formation, previous study has shown that the S isotope evolution of seawater sulfate did not change significantly, and this study took the value of 34‰ (Sahoo et al., 2012 and reference herein). Additionally, large S isotope fractionations were observed in several parts of different sections across the Doushantuo Formation. For instance, in the upper part of the Jiulongwan platform section, the relatively large fractionation of $\Delta^{34}S_{sulfate-pyrite}$ (23.7–47.9‰) with the low $\delta^{34}S_{pyrite}$ values (−2.9 to −16.8‰) indicated sulfate levels greater than 200 μM at the end of the Doushantuo Formation (McFadden et al., 2008; Li et al., 2010). Moreover, the middle enriched part of the Wuhe section demonstrates potentially large $\Delta^{34}S_{sulfate-pyrite}$ (37.0–38.6‰) with low $\delta^{34}S_{pyrite}$ values (−3.7 to −5.3‰), which also indicated high concentrations of sulfate (>200 μM) accumulated during the middle of the Doushantuo Formation (Electronic Appendix Table 1). In the same way, another study, which included the lower part of the black shale samples in the Taoying, Wuhe slope, and basin Yuanjia sections, also exhibited a potential maximum $\Delta^{34}S_{sulfate-pyrite}$ exceeding 65‰ and negative $\delta^{34}S_{py}$ values (−17.2 to −34.9‰), which are also indicative of at least 1 mM sulfate concentrations at the beginning of the Doushantuo Formation (Sahoo et al., 2012). Overall, these large S isotope fractionations with ^{34}S-depleted pyrites might have resulted in BSR processes, and they further indicate that high sulfate concentrations had already accumulated not only at the ending but also at the middle and beginning of the platform, slope and even some basin locations across the Doushantuo Formation.

For the redox-sensitive elements (Mo and U) and Fe speciation, it should not be overlooked that a large amount of H_2S is produced during BSR processes, which could result in a euxinic water column and is necessary for the competitive fixation of significant authigenic Mo–U enrichment (Tribovillard et al., 2006) and the formation of pyrite. It also should be noted that the above-mentioned parts with large S isotope fractionation exhibited strongly authigenic Mo–U enrichment and high Fe_{py}/Fe_{HR} ratios (Figs. 2 and 3; McFadden et al., 2008; Li et al., 2010; Sahoo et al., 2012). In addition, large S isotope fractionations with BSR processes were also observed in some euxinic marine settings,

such as the Black Sea and the Cariaco Basin (Brunner and Bernasconi, 2005; Canfield et al., 2010). Therefore, this consistency in the geochemical data may be related to BSR processes.

With respect to C isotopes, it is well known that pronounced negative $\delta^{13}C_{carb}$ excursions occurred during the Ediacaran sedimentary sequences (Fike et al., 2006; Kaufman et al., 2007; Jiang et al., 2011). For the Doushantuo Formation, these negative $\delta^{13}C_{carb}$ excursions were likely ascribed to the oxidation of the deep oceanic DOC reservoir (Fike et al., 2006; Jiang et al., 2007, 2011; McFadden et al., 2008). There were three distinctive $\delta^{13}C_{carb}$ excursions in the platform section (e.g., the Jiulongwan section; McFadden et al., 2008; Jiang et al., 2011), whereas entirely negative values were present in the slope and basin sections (e.g., the Wuhe and Yuanling sections; Jiang et al., 2011). If the large DOC reservoir existed, the oxidation by sulfate-reducing bacteria through BSR processes could be related to the negative $\delta^{13}C_{carb}$ anomalies under anoxic conditions (Rothman et al., 2003).

Comprehensive consideration of the above geochemical processes indicated a possible link where the BSR processes involving the DOC reservoir and sulfate-reducing bacteria (BSR process: $SO_4^{2-} + 2CH_2O \rightarrow H_2S + 2HCO_3^-$) under euxinic conditions with open system, could result in negative $\delta^{13}C_{carb}$ anomalies, large S isotope fractionation with ^{34}S-depleted sulfide, high Fe_{py}/Fe_{HR} ratios and significant authigenic Mo–U enrichment. In turn, these consistent geochemical results indicate that high sulfate concentrations are associated with gradually oxidative weathering of sulfides by atmospheric oxygen on land. However, the situation might be uncertain and complicated under the ferruginous condition where iron and molybdenum could compete for the free H_2S produced by BSR processes. On the other hand, the oxidation of the DOC reservoir by dissolved free oxygen would also result in the negative δ^{13}Ccarb anomalies, but be accompanied by the absence of authigenic Mo-U enrichment, and the irregular S isotope fractionation and Fepy/FeHR ratios under oxic/suboxic conditions.

5.3.2. Dynamic evolution of the Ediacaran ocean and progressive atmospheric oxygenation

Combining the possible link between the geochemical data described above with the inferred redox conditions from the authigenic Mo and U enrichment, the Fe speciation and S isotopes in this study suggest that the Doushantuo Formation might have undergone at least three stages of evolution during the sedimentary period (Fig. 7).

In *Stage 1*, the limited euxinic condition was the main characteristic of the Doushantuo Formation, which showed a stratified ocean at this stage. At the same time, high sulfate inputs arrived at both the Jiulongwan platform and the Wuhe slope locations, or even at some basins (Yuanjia and Xiangtan sections) (Figs. 2, 3, 4, 7).

Specifically, the Jiulongwan platform section might have been deposited under suboxic conditions above the chemocline, whereas the Xiangtan basin section may have been deposited under anoxic conditions with an intermittent euxinic water column. However, the Wuhe slope section may have been deposited during euxinic to suboxic conditions because of the fluctuating chemocline. The geochemical data and explanations were fairly clear in this stage. 1) In the lower part of the Jiulongwan section, the Mo and U relationships were consistent with suboxic conditions. Positive $\delta^{13}C_{carb}$ values and small S isotope fractionation in this stage might be associated with the absence of activities by sulfate-reducing bacteria under suboxic conditions, rather than with the lower sulfate levels. However, high Fe_{py}/Fe_{HR} values greater than 0.7 might result from the diagenetic processes in this stage (Figs. 2, 6 and 7). 2) Significant authigenic Mo–U enrichment, high Fe_{py}/Fe_{HR} values greater than 0.7 and potentially large $\Delta^{34}S_{sulfate-pyrite}$ values (exceeding 65‰, Sahoo et al., 2012) of the lower enriched part of the Wuhe section indicated that the presence of euxinic conditions with BSR processes is in response to high sulfate inputs at the slope location at this stage. The oxidation of the DOC reservoir by sulfate-reducing bacteria could have led to the negative $\delta^{13}C_{carb}$ anomalies in the lower enriched part. However, the subsequently lower depleted part of the Wuhe section, with negligible Mo–U concentrations, irregular Fe_{py}/Fe_{HR} values and S isotope fractionation, indicated that euxinic conditions had been converted to suboxic conditions due to the descending chemocline. The negative $\delta^{13}C_{carb}$ values of this lower depleted part could be a result of the oxidation of the upwelling DOC by dissolved free oxygen under suboxic conditions (Figs. 3, 6 and 7). 3) Although there are no C isotope data for the Xiangtan basin section, the occasional authigenic Mo–U enrichment and a few high Fe_{py}/Fe_{HR} values indicated that this deep oceanic location was anoxic but perhaps intermittently had a euxinic water column (Figs. 4, 6 and 7). However, another basin section (Yuanjia), with significant authigenic Mo–U enrichment, high Fe_{py}/Fe_{HR} values and potentially large S isotope fractionation (Sahoo et al., 2012), might indicate euxinic conditions and high sulfate input at basin locations in this stage. In summary, the limited occurrence of euxinic conditions and the scope of oceanic sulfate input in this stage demonstrated a preliminary scenario for the Ediacaran ocean–atmosphere system.

In *Stage 2*, a transient euxinic condition occurred in the Wuhe slope in response to the fluctuating chemocline and the continuous sulfate input and atmospheric oxygenation (Fig. 7). However, the sedimentary conditions of the Jiulongwan and Xiangtan sections may not have changed significantly in this stage.

The detailed descriptions were as follows. 1) The Jiulongwan section still lies above the chemocline and was maintained in a suboxic condition at this stage. Furthermore, the relatively small S isotope fractionation suggests that the seemingly impossible BSR processes were present in this stage, which is compatible with the suboxic conditions. Similar to Stage 1, the high Fe_{py}/Fe_{HR} values may have resulted from the diagenetic processes. However, the oxidation of the upwelling DOC with dissolved oxygen in the suboxic condition might be responsible for the short-term negative $\delta^{13}C_{carb}$ excursion (EN2, McFadden et al., 2008; Figs. 2, 6 and 7). 2) In regard to the middle part of the Wuhe section, the redox conditions of the water column in this stage were similar to those of Stage 1. That is to say, the euxinic condition for the middle enriched part and the suboxic condition for the middle depleted part were still attributable to the fluctuating chemocline. Similar to Stage 1, the negative $\delta^{13}C_{carb}$ anomalies resulted from different oxidation mechanisms, such as BSR processes for the middle enriched part, and dissolved free oxygen for the middle depleted part (Figs. 3, 6 and 7). 3) The middle part of the Xiangtan section was deposited under anoxic conditions with an intermittently euxinic water column. The distributions of authigenic Mo–U enrichment indicate a fluctuant oceanic chemistry in the middle to upper part of the Xiangtan section (Figs. 4, 6 and 7). To summarize, the occurrence of euxinic conditions was associated with the presence of BSR processes and high sulfate supplementation in this stage.

In *Stage 3*, the prevailing euxinic conditions dominated in the upper parts of the Jiulongwan and Wuhe sections, but anoxic ferruginous conditions existed in the Xiangtan section at the end of the Doushantuo Formation (Fig. 7). In this stage, the uplifted chemocline brought not only the slope locations but also the platform locations under euxinic conditions. These euxinic conditions might indicate intense BSR processes with high oceanic sulfate supplementation, which could be associated with the continuous oxygenation of the atmosphere during the late Doushantuo period (e.g., Li et al., 2010; McFadden et al., 2008; Fig. 7). Despite the absence of S isotope data for the Wuhe sections, the large S isotope fractionation and high Fe_{py}/Fe_{HR} values of the Jiulongwan section suggest that the presence of BSR processes associated with continuous oceanic sulfate input could have resulted in euxinic conditions. That is as would be expected: the negative $\delta^{13}C_{carb}$ anomalies in the upper parts of the Jiulongwan and Wuhe sections may have been caused by oxidation of the upwelling DOC by oceanic sulfate through bacterial sulfate reduction process in this stage. However, the modest authigenic Mo–U enrichment, modest Fe_{py}/Fe_{HR} and S isotope fractionation in the upper part of the Xiangtan section indicated ferruginous conditions where the H_2S produced by the BSR processes might be insufficient for the fixation of excessive iron.

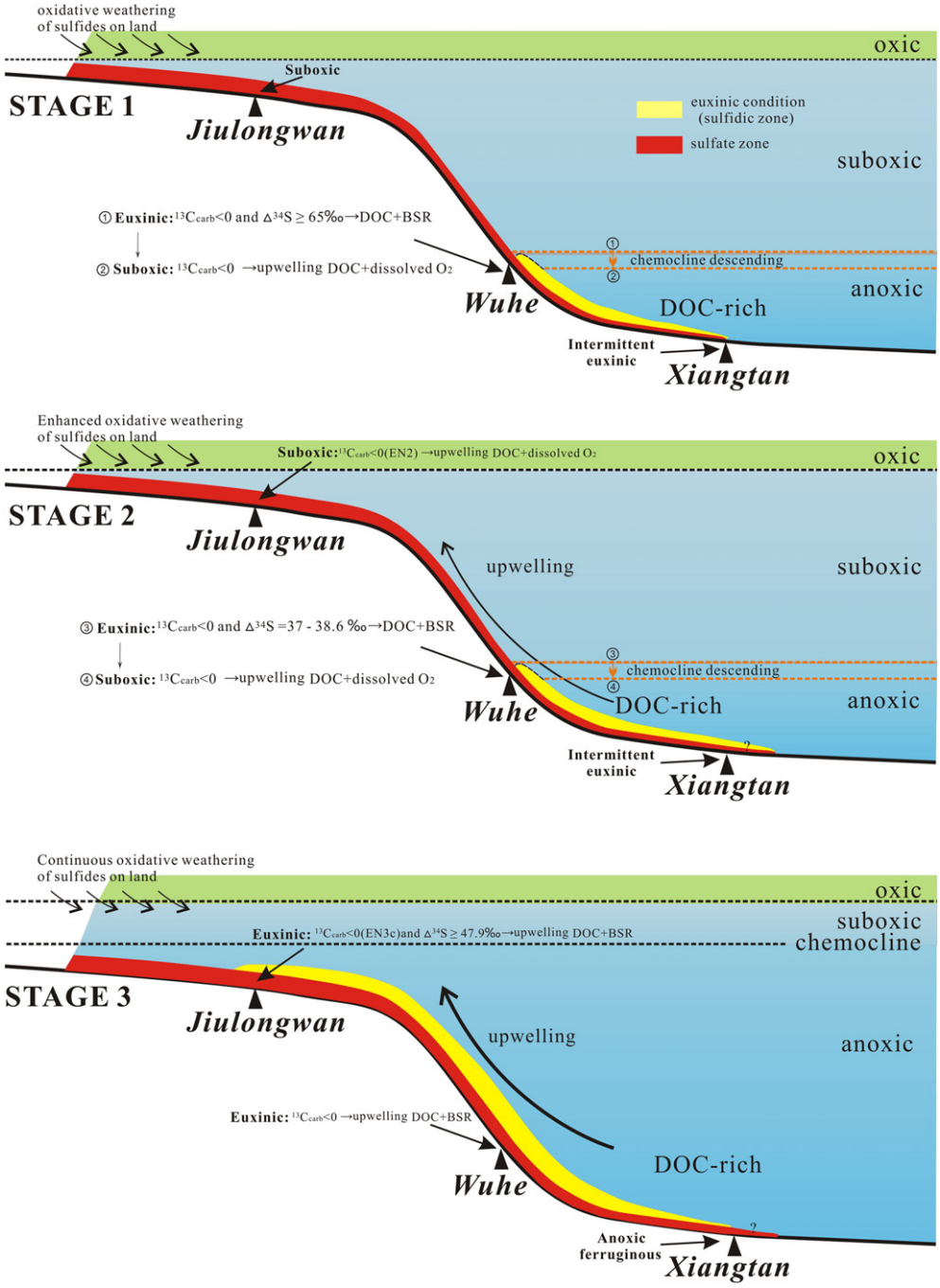

Fig. 7. Schematic diagram of the dynamic evolution of the Ediacaran Doushantuo Formation, South China. In Stage 1, limited euxinic condition occurred near or below the Wuhe slope location, high or sufficient oceanic sulfate concentrations may have accumulated at the platform, slope and some basin locations. In Stage 2, a transient euxinic condition occurred in the Wuhe slope in response to the fluctuating chemocline which is similar to Stage 1. However, other deeper locations below the Xiangtan location are unidentified in this study. In Stage 3, the prevailing euxinic conditions dominated in the upper parts of the Jiulongwan and Wuhe sections, but anoxic ferruginous conditions existed in the Xiangtan section because of the uplifted chemocline associated with the sufficient oceanic sulfate input in response to continuous atmospheric oxygenation at the end of the Doushantuo Formation. The negative $^{13}C_{carb}$ excursions of the Jiulongwan and Wuhe sections are from Jiang et al. (2011) and McFadden et al. (2008). The $\Delta^{34}S_{sulfate-pyrite} \geq 65‰$ of Wuhe section in Stage 1 is from Sahoo et al. (2012) and $\Delta^{34}S_{sulfate-pyrite} \geq 47.9‰$ of Jiulongwan section in Stage 3 is from McFadden et al. (2008) and Li et al. (2010). The symbols of EN2 and EN3c are consistent with McFadden et al. (2008).

6. Conclusions

The investigation of authigenic Mo–U enrichment, together with Fe speciation and S isotopes in the Jiulongwan, Wuhe and Xiangtan sections, suggests distinctive oceanic redox conditions across the platform, slope and basin sections of the Doushantuo Formation. In the Jiulongwan platform section, suboxic conditions characterized the lower part, whereas euxinic conditions were observed in the upper part. Simultaneously, in the Wuhe slope section, three transient euxinic episodes occurred in the lower, middle and upper parts, and the remainder was deposited under suboxic conditions due to the fluctuating chemocline. However, the Xiangtan basin section was characterized by anoxic ferruginous conditions with an intermittently euxinic water column. Furthermore, our investigation of multiple geochemical results was compatible with other published geochemical data indicating a possible link. Specifically, significant authigenic Mo–U enrichment, together with negative $\delta^{13}C_{carb}$ anomalies and large S isotope fractionation and high Fe_{py}/Fe_{HR} ratios, might be associated with the oxidation

of DOC by sufficient sulfate through BSR processes under euxinic conditions, whereas the situation might be complicated and different under ferruginous conditions. Conversely, the absence of significant authigenic Mo–U enrichment, together with negative $\delta^{13}C_{carb}$ anomalies and irregular S isotope fractionation and Fe_{py}/Fe_{HR} ratios, could be related to the oxidation of DOC by dissolved free oxygen under suboxic conditions. Finally, the euxinic/intermittent euxinic conditions across the Doushantuo Formation responded to a dynamic evolution of stratified ocean and progressive atmospheric oxygenation during the early Ediacaran Period.

Supplementary data to this article can be found online at http://dx.doi.org/10.1016/j.chemgeo.2015.09.021.

Acknowledgments

This project is supported by the National Basic Research Program of China(2014CB440906), the 12th Five-year Plan project of the State Key Laboratory of Ore Deposit Geochemistry, Chinese Academy of Sciences (SKLODG-ZY125-07), National Natural Science Foundation of China (Grant Nos. 41273024, 41303039), Youth Innovation Promotion Association CAS and "West Light" of the Chinese Academy of Sciences. We give many thanks to Prof. Li Chao and Dr. Zhang Zihu for determining the Fe speciation and S isotope, to Dr. Bin Yan, Feifei Zhang for helping in the field work, to the anonymous reviewers for reviewing the manuscript, and to the editor for their comments and the editorial handling.

References

Ader, M., Macouin, M., Trindade, R.I.F., Hadrien, M.-H., Yang, Z., Sun, Z., Besse, J., 2009. A multilayered water column in the Ediacaran Yangtze platform? Insights from carbonate and organic matter paired $\delta^{13}C$. Earth Planet. Sci. Lett. 288, 213–227.

Ader, M., Sansjofre, P., Halverson, G.P., Busigny, V., Trindade, R.I.F., Kunzmann, M., Nogueira, A.C.R., 2014. Ocean redox structure across the late Neoproterozoic Oxygenation Event: a nitrogen isotope perspective. Earth Planet. Sci. Lett. 396, 1–13.

Algeo, T.J., Maynard, J.B., 2004. Trace-element behavior and redox facies in core shales of upper Pennsylvanian Kansas-type cyclothems. Chem. Geol. 206, 289–318.

Algeo, T.J., Tribovillard, N., 2009. Environmental analysis of paleoceanographic systems based on molybdenum–uranium covariation. Chem. Geol. 268, 211–225.

Anderson, R.F., Fleischer, M.Q., LeHuray, A.P., 1989. Concentration, oxidation state and particle flux of uranium in the Black Sea. Geochim. Cosmochim. Acta 53, 2215–2224.

Bjerrum, C.J., Canfield, D.E., 2011. Towards a quantitative understanding of the late Neoproterozoic carbon cycle. Proc. Natl. Acad. Sci. 108, 5542–5547.

Brunner, B., Bernasconi, S.M., 2005. A revised isotope fractionation model for dissimilatory sulfate reduction in sulfate reducing bacteria. Geochim. Cosmochim. Acta 69, 4759–4771.

Calver, C.R., 2000. Isotope stratigraphy of the Ediacarian (Neoproterozoic III) of the Adelaide rift complex, Australia, and the overprint of water column stratification. Precambrian Res. 100, 121–150.

Campbell, I.H., Squire, R.J., 2010. The mountains that triggered the Late Neoproterozoic increase in oxygen: the second great oxidation event. Geochim. Cosmochim. Acta 74, 4187–4206.

Canfield, D.E., 1998. A new model for Proterozoic ocean chemistry. Nature 396, 450–453.

Canfield, D.E., 2005. The early history of atmospheric oxygen: homage to Robert M. Garrels. Annu. Rev. Earth Planet. Sci. 33, 1–36.

Canfield, D.E., Teske, A., 1996. Late Proterozoic rise in atmospheric oxygen concentration inferred from phylogenetic and sulphur-isotope studies. Nature 382, 127–132.

Canfield, D.E., Thamdrup, B., 1994. The production of ^{34}S-depleted sulfide during bacterial disproportionation of elemental sulfur. Science 266, 1973–1975.

Canfield, D.E., Habicht, K.S., Thamdrup, B., 2000. The Archean sulfur cycle and the early history of atmospheric oxygen. Science 288, 658–661.

Canfield, D.E., Poulton, S.W., Narbonne, G.M., 2007. Late-Neoproterozoic deep-ocean oxygenation and the rise of animal life. Science 315, 92–95.

Canfield, D.E., Poulton, S.W., Knoll, A.H., Narbonne, G.M., Ross, G., Godlberg, T., Strauss, H., 2008. Ferruginous conditions dominated later-Neoproterozoic deep-water chemistry. Science 321, 949–952.

Canfield, D.E., Farquhar, J., Zerkle, A.L., 2010. High isotope fractionations during sulfate reduction in a low-sulfate euxinic ocean analog. Geology 38, 415–418.

Chaillou, G., Anschutz, P., Lavaux, G., Schäfer, J., Blanc, G., 2002. The distribution of Mo, U, and Cd in relation to major redox species in muddy sediments of the Bay of Biscay. Mar. Chem. 80, 41–59.

Condon, D., Zhu, M., Bowring, S., Wang, W., Yang, A., Jin, Y., 2005. U–Pb ages from the Neoproterozoic Doushantuo Formation, China. Science 2005 (308), 95–98.

Crusius, J., Calvert, S., Pedersen, T., Sage, D., 1996. Rhenium and molybdenum enrichments in sediments as indicators of oxic, suboxic, and sulfidic conditions of deposition. Earth Planet. Sci. Lett. 145, 65–78.

Erickson, B.E., Helz, G.R., 2000. Molybdenum (VI) speciation in sulfidic waters: stability and lability of thiomolybdates. Geochim. Cosmochim. Acta 64, 1149–1158.

Fan, H., Zhu, X., Wen, H., Yan, B., Li, J., Feng, L., 2014. Oxygenation of Ediacaran ocean recored by iron isotopes. Geochim. Cosmochim. Acta 140, 80–94.

Fike, D.A., Grotzinger, J.P., Pratt, L.M., Summons, R.E., 2006. Oxidation of the Ediacaran Ocean. Nature 444, 744–747.

Frei, R., Gaucher, C., Poultion, S.W., Canfield, D.E., 2009. Fluctuations in Precambrian atmospheric oxygenation recorded by chromium isotopes. Nature 461, 250–253.

Grotzinger, J.P., Knoll, A.H., 1995. Anomalous carbonate precipitates: is the Precambrian the key to the Permian? Palaios 10, 578–596.

Guo, Q., Strauss, H., Zhu, M., Zhang, J., Yang, X., Lu, M., Zhao, F., 2011. High resolution organic carbon isotope stratigraphy from a slope to basinal setting on the Yangtze platform, South China: implications for the Ediacaran–Cambrian transition. Precambrian Res. 225, 209–217.

Habicht, K.S., Canfield, D.E., 2001. Isotope fractionation by sulfate-reducing natural populations and the isotopic composition of sulfide in marine sediments. Geology 29, 555–558.

Habicht, K.S., Gade, M., Thamdrup, B., Berg, P., Canfield, D.E., 2002. Calibration of sulfate levels in the Archean ocean. Science 298, 2372–2374.

Halverson, G.P., Hurtgen, M.T., 2007. Ediacaran growth of the marine sulfate reservoir. Earth Planet. Sci. Lett. 263, 32–44.

Halverson, G.P., Hoffman, P.F., Schrag, D.P., Maloof, A.C., Rice, A.H.N., 2005. Toward a Neoproterozoic composite carbon-isotope record. Geol. Soc. Am. Bull. 117, 1181–1207.

Helz, G.R., Miller, C.V., Charnock, J.M., Mosselmans, J.L.W., Pattrick, R.A.D., Garner, C.D., Vaughan, D.J., 1996. Mechanisms of molybdenum removal from the sea and its concentration in black shales: EXAFS evidences. Geochim. Cosmochim. Acta 60, 3631–3642.

Higgins, J.A., Schrag, D.P., 2006. Beyond methane: towards a theory for the Paleocene–Eocene thermal maximum. Earth Planet. Sci. Lett. 245, 523–537.

Hoffman, P.F., Schrag, D.P., 2002. The snowball earth hypothesis: testing the limits of global change. Terra Nova 14, 129–155.

Hoffman, P.F., Kaufman, A.J., Halverson, G.P., Schrag, D.P., 1998. A Neoproterozoic snowball earth. Science 281, 1342–1346.

Hurtgen, M.T., Arthur, M.A., Halverson, G.P., 2005. Neoproterozoic sulfur isotopes, the evolution of microbial sulfur species, and the burial efficiency of sulfide as sedimentary pyrite. Geology 33, 41–44.

Jiang, G., Christie-Blick, N., Kaufman, A.J., Banerjee, D.M., Rai, V., 2002. Sequence stratigraphy of the Neoproterozoic Infra Krol Formation and Krol Group, Lesser Himalaya, India. J. Sediment. Res. 72, 524–542.

Jiang, G., Kennedy, M.J., Christie-Blick, N., 2003. Stable isotopic evidence for methane seeps in Neoproterozoic postglacial cap carbonates. Nature 426, 822–826.

Jiang, G., Shi, X., Zhang, S., 2006a. Methane seeps, methane hydrate destabilization, and the late Neoproterozoic postglacial cap carbonates. Chin. Sci. Bull. 51, 1152–1173.

Jiang, G., Kennedy, M.J., Christie-Blick, N., Wu, H., Zhang, S., 2006b. Stratigraphy, sedimentary structures, and textures of the late Neoproterozoic Doushantuo cap carbonate in South China. J. Sediment. Res. 76, 978–995.

Jiang, G., Kaufman, A.J., Christie-Blick, N., Zhang, S., Wu, H., 2007. Carbon isotope variability across the Ediacaran Yangtze platform in South China: implications for a large surface-to-deep ocean $\delta^{13}C$ gradient. Earth Planet. Sci. Lett. 261, 303–320.

Jiang, G., Shi, X., Zhang, S., Wang, Y., Xiao, S., 2011. Stratigraphy and paleogeography of the Ediacaran Doushantuo Formation (ca. 635–551 Ma) in South China. Gondwana Res. 19, 831–849.

Kaufman, A.J., Hayes, J.M., Knoll, A.H., Germs, G.J.B., 1991. Isotopic compositions of carbonates and organic carbon from upper Proterozoic successions in Namibia; stratigraphic variation and the effects of diagenesis and metamorphism. Precambrian Res. 49, 301–327.

Kaufman, A.J., Corsetti, F.A., Varni, M.A., 2007. The effect of rising atmospheric oxygen on carbon and sulfur isotope anomalies in the Neoproterozoic Johnnie Formation, Death Valley, USA. Chem. Geol. 237, 47–63.

Kendall, B., Komiya, T., Lyons, T.W., Bates, S.M., Gordon, G.W., Romaniello, S.J., Jiang, G.Q., Creaser, R.A., Xiao, S.H., McFadden, K., Sawaki, Y., Tahata, M., Shu, D.G., Han, J., Li, Y., Chu, X.L., Anbar, A.D., 2015. Uranium and molybdenum isotope evidence for an episode of widespread ocean oxygenation during the late Ediacaran Period. Geochim. Cosmochim. Acta 156, 173–193.

Kennedy, M.J., Christie-Blick, N., Sohl, L.E., 2001. Are Proterozoic cap carbonates and isotopic excursions a record of gas hydrate destabilization following Earth's coldest intervals? Geology 29, 443–446.

Klinkhammer, G.P., Palmer, M.R., 1991. Uranium in the oceans: where it goes and why. Geochim. Cosmochim. Acta 55, 1799–1806.

Knoll, A.H., Bambach, R.K., Canfield, D.E., Grotzinger, J.P., 1996. Comparative earth history and Late Permian mass extinction. Science 273, 452–457.

Le Guerroué, E., Cozzi, A., 2010. Veracity of Neoproterozoic negative C-isotope values: the termination of the Shuram negative excursion. Gondwana Res. 17, 653–661.

Li, C., Love, G.D., Lyons, T.W., Fike, D.A., Sessions, A.L., Chu, X., 2010. A stratified redox model for the Ediacaran ocean. Science 328, 80–83.

McFadden, K.A., Huang, J., Chu, X., Jiang, G., Kaufman, A.J., Zhou, C., Yuan, X., Xiao, S., 2008. Pulsed oxidation and biological evolution in the Ediacaran Doushantuo Formation. Proc. Natl. Acad. Sci. 105, 3197–3202.

Och, L.M., Shields-Zhou, G.A., 2012. The Neoproterozoic oxygenation event: environmental perturbations and biogeochemical cycling. Earth-Sci. Rev. 110, 26–57.

Qi, L., Hu, J., Gregoire, D.C., 2000. Determination of trace elements in granites by inductively coupled plasma mass spectrometry. Talanta 51, 507–513.

Partin, C.A., Bekker, A., Planavsky, N.J., Scott, C.T., Gill, B.C., Li, C., Podkovyrov, V., Maslov, A., Konhauser, K.O., Lalonde, S.V., Love, G.D., Poulton, S.W., Lyons, T.W., 2013. Large-scale fluctuations in Precambrian atmospheric and oceanic oxygen levels from the record of U in shales, Earth Planet. Sci. Lett. 369–370, 284–293.

Poulton, S.W., Canfield, D.E., 2011. Ferruginous conditions: A dominant feature of the ocean through Earth's history. Elements 7, 107–112.

Rothman, D.H., Hayes, J.M., Summons, R.E., 2003. Dynamics of the Neoproterozoic carbon cycle. Proc. Natl. Acad. Sci. 100, 8124–8129.
Raiswell, R., Newton, R., Bottrell, S.H., Coburn, P.M., Briggs, D.E.G., Bond, D.P.G., Poulton, S.W., 2008. Turbidite depositional influences on the diagenesis of Beecher's Trilobite Bed and the Hunsruck Slate; Sites of soft tissue pyritization. AM. J. Sci. 308, 105–129.
Sahoo, S.K., Planavsky, N.J., Kendall, B., Wang, X., Shi, X., Scott, C., Anbar, A.D., Lyons, T.W., Jiang, G., 2012. Ocean oxygenation in the wake of the Marinoan glaciation. Nature 489, 546–549.
Schröder, S., Grotzinger, J.P., 2007. Evidence for anoxia at the Ediacaran–Cambrian boundary: the record of redox-sensitive trace elements and rare earth elements in Oman. J. Geol. Soc. 164, 175–187.
Scott, C., Lyons, T.W., 2012. Contrasting molybdenum cycling and isotopic properties in euxinic versus non-euxinic sediments and sedimentary rocks: refining the paleoproxies. Chem. Geol. 324-325, 19–27.
Scott, C., Lyons, T.W., Bekker, A., Shen, Y., Poulton, S.W., Chu, X., Anbar, A.D., 2008. Tracing the stepwise oxygenation of the Proterozoic ocean. Nature 452, 456–459.
Shen, Y., Zhang, T., Hoffman, P.F., 2008. On the coevolution of Ediacaran oceans and animals. Proc. Natl. Acad. Sci. 105, 7376–7381.
Shields, G.A., 2005. Neoproterozoic cap carbonates: a critical appraisal of existing models and the plumeworld hypothesis. Terra Nova 17, 299–310.
Shields, G.A., 2007. A normalised seawater strontium isotope curve: possible implications for Neoproterozoic–Cambrian weathering rates and the further oxygenation of the earth. eEarth 2, 35–42.
Taylor, S.R., McLennan, S.M., 1985. The Continental Crust: Its Composition and Evolution. Blackwell, Oxford (312 pp.).
Tribovillard, N., Desprairies, A., Lallier-Vergès, E., Moureau, N., Ramdani, A., Ramanampisoa, L., 1994. Geochemical study of organic-rich cycles from the Kimmeridge Clay Formation of Yorkshire (G.B.): productivity vs. anoxia. Palaeogeogr. Palaeoclimatol. Palaeoecol. 108, 165–181.
Tribovillard, N., Riboulleau, A., Lyons, T., Baudin, F., 2004. Enhanced trapping of molybdenum by sulfurized marine organic matter of marine origin in Mesozoic limestones and shales. Chem. Geol. 213, 385–401.
Tribovillard, N., Algeo, T.J., Lyons, T., Riboulleau, A., 2006. Trace metals as paleoredox and paleoproductivity proxies: an update. Chem. Geol. 232, 12–32.
Tribovillard, N., Algeo, T.J., Baudin, F., Riboulleau, A., 2012. Analysis of marine environmental conditions based on molybdenum–uranium covariation—applications to Mesozoic paleoceanography. Chem. Geol. 324-325, 46–58.
Vorlicek, T.P., Helz, G.R., 2002. Catalysis by mineral surfaces: implications for Mo geochemistry in anoxic environments. Geochim. Cosmochim. Acta 66, 3679–3692.
Vorlicek, T.P., Kahn, M.D., Kasuza, Y., Helz, G.R., 2004. Capture of molybdenum in pyrite-forming sediments: role of ligand-induced reduction by polysulfides. Geochim. Cosmochim. Acta 68, 547–556.
Wang, L., 2012. Paleo-oceanic redox conditions during deposition of the Ediacaran Doushantuo Formation in South China (A dissertation submitted to China University of Geosciences, Beijing for a doctor degree. Beijing (in Chinese with English abstract)).
Wang, L., Shi, X., Jiang, G., 2012. Pyrite morphology and redox fluctuations recorded in the Ediacaran Doushantuo Formation. Palaeogeogr. Palaeoclimatol. Palaeoecol. 254 (217–228), 333 (218–227).
Wood, R.A., Poulton, S.W., Prave, A.R., Hoffmann, K.-H., Clarkson, M.O., Guibaud, R., Lyne, J.W., Tostevin, R., Bowyer, F., Penny, A.M., Curtis, A., Kasemann, S.A., 2015. Dynamic redox conditions control late Ediacaran metazoan ecosystems in the Nama Group, Namibia. Precambrian Res. 261, 252–271.
Xiao, S., Laflamme, M., 2008. On the eve of animal radiation: phylogeny, ecology and evolution of the Ediacara biota. Trends Ecol. Evol. 24, 31–40.
Xiao, S., Yuan, X., Steiner, M., Knoll, A.H., 2002. Macroscopic carbonaceous compressions in a terminal Proterozoic shale: a systematic reassessment of the Miaohe biota, South China. J. Paleontol. 76, 347–376.
Xiao, S., McFadden, K.A., Peek, S., Kaufman, A.J., Zhou, C., Jiang, G., Hu, J., 2012. Integrated chemostratigraphy of the Doushantuo Formation at the northern Xiaofenghe section (Yangtze Gorges, South China) and its implication for Ediacaran stratigraphic correlation and ocean redox models. Precambrian Res. 192-195, 125–141.
Zhao, Y., Chen, M., Peng, J., Yu, M., He, M., Wang, Y., Yang, R., Wang, P., Zhang, Z., 2004. Discovery of a Miaohe-type biota from the Neoproterozoic Doushantuo Formation in Jiangkou County, Guizhou province, China. Chin. Sci. Bull. 49, 2224–2226.
Zheng, Y., Anderson, R.F., van Geen, A., Kuwabara, J., 2000. Authigenic molybdenum formation in marine sediments: a link to pore water sulfide in the Santa Barbara Basin. Geochim. Cosmochim. Acta 64, 4165–4178.
Zhou, C., Xiao, S., 2007. Ediacaran $\delta^{13}C$ chemostratigraphy of South China. Chem. Geol. 237, 89–108.
Zhou, C., Xie, G., McFadden, K., Xiao, S., Yuan, X., 2007. The diversification and extinction of Doushantuo–Pertatataka acritarchs in South China: causes and biostratigraphic significance. Geol. J. 42, 229–262.
Zhu, M., Zhang, J., Yang, A., 2007. Integrated Ediacaran (Sinian) chronostratigraphy of South China. Palaeogeogr. Palaeoclimatol. Palaeoecol. 254, 7–61.
Zhu, M., Lu, M., Zhang, J., Zhao, F., Li, G., Yang, A., Zhao, X., Zhao, M., 2013. Carbon isotope chemostratigraphy and sedimentary facies evolution of the Ediacaran Doushantuo Formation in western Hubei, South China. Precambrian Res. 225, 7–28.